

SATURATION EFFECTS IN DIS AT LOW x^*

K. GOLEC-BIERNAT

II Institute of Theoretical Physics, University of Hamburg
Luruper Chaussee 149, 22761 Hamburg, Germany

and

H. Niewodniczański Institute of Nuclear Physics
Radzikowskiego 152, 31-342 Kraków, Poland*(Received July 16, 2002)*

We review basic ideas related to saturation of parton densities at small value of the Bjorken variable x . A special emphasis is put on interpreting the results from the ep deep inelastic scattering experiments at HERA.

PACS numbers: 13.60.Hb, 12.38.Bx

1. Introduction

The idea of parton saturation naturally arises in Deep Inelastic Scattering (DIS) at small values of the Bjorken variable x , studied currently at the HERA collider in DESY. The main measured small- x effect is a strong rise of the proton structure function F_2 in the limit $x \rightarrow 0$ for fixed virtuality Q^2 . Interpreted with the help of linear evolution equations of Quantum Chromodynamics, this is a reflection of increasing parton densities (sea quarks and gluons). Formally, the parton rise is so strong that for sufficiently small x the computed cross section violates unitarity, which signals that important physical effects were neglected in the approximation leading to the linear evolution equations. These effects are responsible for *saturation* of the parton densities by taming their strong rise. Whether the saturation effects are already visible in the F_2 at HERA is disputable, the linear DGLAP evolution equations describe the data for $Q^2 > 2 \text{ GeV}^2$. However, more exclusive diffractive processes strongly hint towards the affirmative answer to the posed question. Moreover, the transition region of $Q^2 \simeq 1 \text{ GeV}^2$ for F_2 , where the DGLAP analysis encounters basic difficulties, is easily described

* Plenary presentation at the X International Workshop on Deep Inelastic Scattering (DIS2002) Cracow, Poland, 30 April–4 May, 2002.

within an approach based on parton saturation. An important result of saturation is the existence of a saturation scale which is reflected in a new scaling law for inclusive DIS cross section. The small- x data do really show such a regularity.

In the following we present basic concepts leading to the notion of parton saturation and discuss the relevance of this effect for experimental data, mainly from HERA.

2. Linear evolution equations

In the standard description of ep DIS the structure function F_2 is determined by the quark and antiquark densities in the proton

$$F_2(x, Q^2) = \sum_f e_f^2 x \left\{ q_f(x, Q^2) + \bar{q}_f(x, Q^2) \right\} + \mathcal{O}(\alpha_s), \quad (1)$$

where the summation is done over quark flavors. As usual, $x = Q^2/(2P \cdot q)$ and $Q^2 = -q^2$, where P and q are the proton and virtual photon momenta. The quark densities together with the gluon density $g(x, Q^2)$ satisfies the DGLAP evolution equations [1]. In the matrix notation, $\mathbf{q} = (q_f, \bar{q}_f, g)$,

$$\frac{\partial \mathbf{q}(x, Q^2)}{\partial \ln Q^2} = \int_x^1 \frac{dz}{z} \mathbf{P}\left(\frac{x}{z}, Q^2\right) \mathbf{q}(z, Q^2), \quad (2)$$

where the matrix of splitting functions is computed perturbatively,

$$\mathbf{P}(z, Q^2) = \alpha_s(Q^2) \mathbf{P}^{(1)}(z) + \alpha_s^2(Q^2) \mathbf{P}^{(2)}(z) + \dots \quad (3)$$

Eq. (2) allows to determine the scale dependence in (1) provided initial conditions at some scale Q_0^2 are given. This is done by fitting their form in x to the existing DIS data. In this way logarithmic scaling violation of F_2 is explained. The above description applies to $Q^2 \gg \Lambda_{\text{QCD}}^2$ for perturbative QCD to be valid. How low in Q^2 and in x the pure DGLAP approach is applicable should be determined from the analysis of data. In principle, the values of x and Q^2 indicating that boundary are correlated, *i.e.* $Q^2 = Q^2(x)$.

The low Q^2 region brings an issue of the $(1/Q^2)^n$ corrections (twist expansion) to F_2 , treated systematically in the operator product expansion of two electromagnetic currents. Eq. (1) takes into account only the logarithmic contribution in this expansion. For moderate x this is a dominant contribution, as shown by successful DGLAP analysis of DIS data. For $x \ll 1$, however, each term in the twist expansion,

$$F_2(x, Q^2) = F_2^{(0)}(x, \ln Q^2) + F_2^{(1)}(x, \ln Q^2) \frac{M^2}{Q^2} + \dots, \quad (4)$$

can be equally important due to the presence of large logarithms $\ln(1/x)$. Thus, a new systematics is necessary allowing to resume these large logarithms in the small- x limit independent of the twist expansion. This is done through the k_{\perp} -factorization formula [2] which contains all twists

$$F_2(x, Q^2) = \int \frac{d^2\mathbf{k}}{k^4} \Phi(Q^2, \mathbf{k}) f(x, \mathbf{k}), \tag{5}$$

where $\Phi(Q^2, \mathbf{k})$ is the virtual photon impact factor describing the process $\gamma^* \rightarrow q\bar{q} \rightarrow \gamma^*$, see Fig. 1. The function $f(x, \mathbf{k})$ is the unintegrated gluon distribution, related to the gluon density at large Q^2 and small x by

$$xg(x, Q^2) = \int \frac{d^2\mathbf{k}}{\pi k^2} f(x, \mathbf{k}) \Theta(Q^2 - k^2). \tag{6}$$

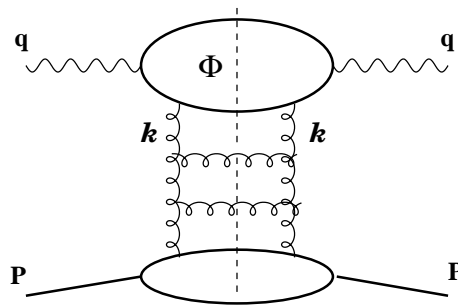


Fig. 1. k_{\perp} -factorization in DIS, Eq. (5).

In the above \mathbf{k} is a two-dimensional vector of transverse momenta of two gluons which couple to the quark loop in four possible ways. Notice the integration over all values of $|\mathbf{k}|$ in (5). This means that the region of small momenta needs special attention to avoid problems with perturbative stability. The unintegrated gluon distribution satisfies the BFKL equation [3] which can be written as an evolution equation in the rapidity $Y = \ln(1/x)$. In the leading order approximation, when the terms proportional to $(\alpha_s \ln(1/x))^n$ are resumed,

$$\frac{\partial f(x, \mathbf{k})}{\partial Y} = \frac{3\alpha_s}{\pi} \int \frac{d^2\mathbf{l}}{\pi l^2} \{f(x, \mathbf{k} + \mathbf{l}) - \Theta(k^2 - l^2) f(x, \mathbf{k})\}. \tag{7}$$

Diagrammatically, the BFKL equation resumes the ladder diagrams with two exchanged (reggeized) gluons interacting through the real gluons in the rungs strongly ordered in rapidity. Each emitted gluon leads to the large logarithm $\alpha_s \ln(1/x)$. Since this is a colorless exchange which gives the dominant behavior at large energy \sqrt{s} of the γ^*p system ($x = Q^2/s$), it is termed the BFKL pomeron.

The solution of Eq. (7) gives the x dependence of F_2 at small x . In the limit $x \rightarrow 0$ and Q^2 fixed, it is given by the azimuthally symmetric saddle point solution

$$\frac{f(x, k^2)}{\sqrt{k^2}} = x^{-12\alpha_s \ln 2/\pi} \frac{\exp\left(\frac{-\ln^2(k^2/k_0^2)}{D}\right)}{\sqrt{\pi D}}, \quad (8)$$

where $D \sim \ln(1/x)$. Thus for decreasing x , the solution features a power-like rise with x and *diffusion* in $\ln k^2$. Even though at some initial $x = x_0$ the solution is concentrated around $k^2 \approx k_0^2$, it diffuses into the region of larger and smaller values of k^2 for $x \rightarrow 0$, see Fig. 2. Diffusion into the infrared region means that the BFKL approximation is strongly sensitive to nonperturbative effects since the cross section might be dominated by a contribution from $|\mathbf{k}| \simeq \Lambda$. This problem can be phenomenologically cured by a separate treatment of the infrared domain. However, infrared diffusion signals fundamental difficulty which reflects incompleteness of the BFKL approximation. This is intimately related to violation of unitarity reflected in the Froissard bound: $F_2 \leq c \ln^2(1/x)$, in contrast to the power-like rise in (8). The next-to-leading corrections to the BFKL equation, see [4] and references therein, weaken the rise but the two discussed problems remain.

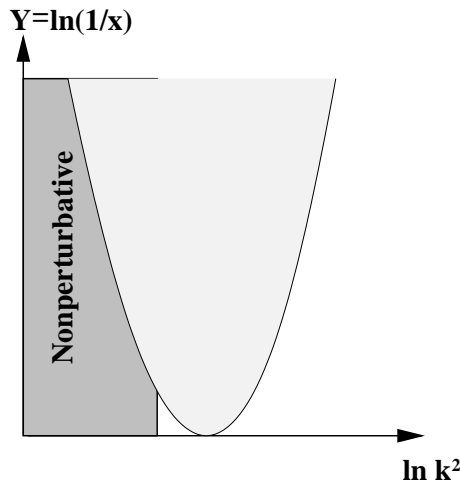


Fig. 2. Diffusion pattern from the BFKL equation.

The missing physical effect in the BFKL approximation is parton saturation. In the infinite momentum frame of the proton, the following picture of this phenomenon exists. The transverse size of gluons with transverse momentum \mathbf{k} is proportional to $1/|\mathbf{k}|$. For large $|\mathbf{k}|$, the BFKL mechanism of

gluon radiation, $g \rightarrow gg$, populates the transverse space with large number (per unit of rapidity) of small size gluons. The same mechanism also applies to large size gluons with small transverse momenta. In this case, however, the BFKL approach is incomplete since large gluons strongly overlap and fusion processes, $gg \rightarrow g$, are equally important. By taking these processes into account unitarity is restored and infrared diffusion cured. The key element for this is the emergence of a rising with rapidity *saturation scale* $Q_s(Y)$, which is a fundamental property of parton saturation [5, 7]. The density of large gluons with $|\mathbf{k}| < Q_s(Y)$ no longer strongly rises and unitarity is restored. The low momentum contribution to the cross section is dominated by $|\mathbf{k}| \simeq Q_s(Y) \gg \Lambda_{\text{QCD}}$ for sufficiently large Y , which allows to avoid the problem of strong sensitivity to the infrared domain. In the forthcoming we show how this idea is realized in practice.

3. The dipole picture

The problem of restoration of unitarity in the description of DIS at small x was pioneered by Gribov, Levin and Ryskin in [5]. In there nonlinear corrections to the DGLAP evolution equations were presented and subsequently rigorously derived in the double logarithmic approximation by Mueller and Qiu in [6]. In this approximation, Q^2 is large and x is small such that terms proportional to $(\alpha_s \ln x \ln Q^2)^n \sim 1$ are resummed. We want to avoid the high Q^2 assumption and approach the problem in the approximation in which the BFKL formulation of DIS was discussed. To this end we transform the k_{\perp} -factorization formula (5) into the Fourier conjugate representation where the transverse momentum \mathbf{k} is traded for its conjugate transverse separation \mathbf{r} . Thus the following formula is found, see *e.g.* [8],

$$F_2 = \frac{Q^2}{4\pi^2\alpha_{em}} (\sigma_T + \sigma_L), \quad (9)$$

and

$$\sigma_{T,L}(x, Q^2) = \int d^2\mathbf{r} dz \left| \Psi_{T,L}(Q^2, \mathbf{r}, z) \right|^2 \hat{\sigma}(\mathbf{r}, x), \quad (10)$$

where $\sigma_{T,L}$ are γ^*p cross sections for the indicated polarizations. Here \mathbf{r} is the $q\bar{q}$ dipole transverse separation and z is the longitudinal momentum fraction of the dipole quark/antiquark with respect to the momentum $q' = q + xp$. The physical interpretation of factorization in (10) is provided in the proton rest frame. The virtual photon γ^* splits into a $q\bar{q}$ pair long before the interaction with the proton since the formation time, $\tau_{q\bar{q}} \sim 1/(xM)$, is very large in the small- x limit. This process is described by the lowest Fock state light-cone wave function of the photon, $\Psi_{T,L}$ [9]. The interaction with the proton is encoded in the $q\bar{q}$ dipole cross section $\hat{\sigma}(\mathbf{r}, x)$.

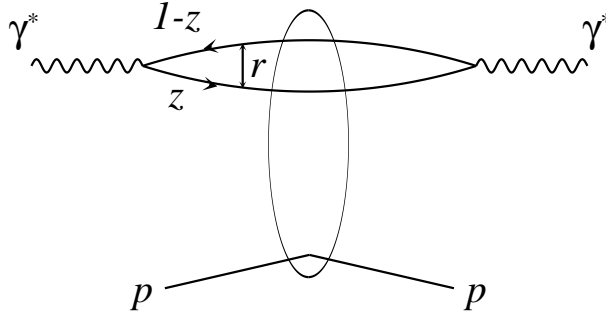


Fig. 3. The illustration of factorization in Eq. (10).

The BFKL approximation has a nice formulation in the dipole picture in the large N_c limit [10, 11]. In this limit, emission of a gluon by a quark can be viewed as a creation of two dipoles out of the parent dipole, see Fig. 4. Each new dipole can radiate a gluon with much softer longitudinal momenta, which leads to new dipoles. In this way the parent $q\bar{q}$ dipole \mathbf{r} evolves into a collection of dipoles \mathbf{r}' with the density $n(\mathbf{r}, \mathbf{r}', x)$. The interaction of each dipole with the proton occurs through exchange of a single perturbative gluon. Thus in this picture the dipole cross section equals

$$\hat{\sigma}(\mathbf{r}, x) = \int d^2\mathbf{r}' n(\mathbf{r}, \mathbf{r}', x) \sigma_{gp}(\mathbf{r}'), \tag{11}$$

where $\sigma_{gp}(\mathbf{r}')$ describes the interaction of a dipole \mathbf{r}' with the proton. The BFKL effects are located in evolution of the photon wave function, the large logarithms $\ln(1/x)$ come from strong ordering of longitudinal momenta of the emitted gluons. Consequently, the dipole density obeys the BFKL equation in the \mathbf{r} -space

$$\frac{\partial n(\mathbf{r}, \mathbf{r}', x)}{\partial Y} = \frac{N_c \alpha_s}{\pi} \int \frac{d^2\boldsymbol{\rho}}{\pi \rho^2} \{ n(\mathbf{r} + \boldsymbol{\rho}, \mathbf{r}', x) - \Theta(\mathbf{r}^2 - \boldsymbol{\rho}^2) n(\mathbf{r}, \mathbf{r}', x) \}. \tag{12}$$

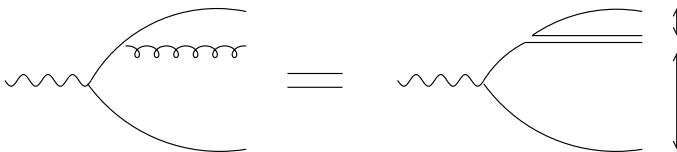


Fig. 4. Emission of a gluon in the large N_c limit.

The variable \mathbf{r}' is a parameter in Eq. (12), thus the dipole cross section (11) obeys the same equation. Notice that the integral kernel on the r.h.s. of Eq. (12) has mathematically the same form as in the BFKL equation in the momentum space (7). Like in the momentum space, the saddle point solution exhibits the power-like rise in x and diffusion in $\ln \mathbf{r}^2$

$$\frac{n(\mathbf{r}, \mathbf{r}', x)}{\sqrt{r^2}} = x^{-4N_c \alpha_s \ln 2/\pi} \frac{\exp(-\ln^2(r^2/r'^2)/D)}{\sqrt{\pi D}} \quad (13)$$

and $D \sim \ln(1/x)$. Now, infrared diffusion corresponds to an unlimited rise of the dipole density for large size parent dipoles.

From (11) and (13), the BFKL dipole cross section behaves as $x^{-\lambda}$ for any r which leads to violation of unitarity when $x \rightarrow 0$ as in the momentum space. Now, the saturation effects would correspond to interactions between dipoles. Before discussing QCD formulations of these effects, we present a phenomenological model which captures essential features of parton saturation and describes the DIS data.

4. The saturation model

In this model [12], the dipole cross section is bounded by an energy independent value σ_0 which assures unitarity of F_2

$$\hat{\sigma}(\mathbf{r}, x) = \sigma_0 \left\{ 1 - \exp\left(-\frac{r^2}{4R_0^2(x)}\right) \right\}, \quad (14)$$

where $R_0(x)$, called saturation radius, is given by

$$R_0(x) = 1 \text{ GeV}^{-1} \left(\frac{x}{x_0}\right)^{\lambda/2}. \quad (15)$$

The three parameters, $\sigma_0 = 23 \text{ mb}$, $\lambda \simeq 0.3$ and $x_0 = 3 \times 10^{-4}$, were fitted to all small- x DIS data with $x < 10^{-2}$. The resulting curves for different values of x are shown in Fig. 5. At small r , $\hat{\sigma}$ features color transparency, $\hat{\sigma} \sim r^2$, which is perturbative QCD phenomenon, while for large r , $\hat{\sigma}$ saturates, $\hat{\sigma} \simeq \sigma_0$. The transition between the two regimes is governed by the increasing with x saturation radius $R_0(x)$. Therefore, an important feature of the model is that *for decreasing x , the dipole cross section saturates for smaller dipole sizes*, see Fig. 5. The BFKL rise with x is encoded in the small r part of $\hat{\sigma}$ since for $r \ll R_0$, $\hat{\sigma} \sim x^{-\lambda}$. In contrast to the BFKL result, however, with decreasing x the saturation radius $R_0(x)$ gets smaller and consequently $\hat{\sigma}$ never exceeds σ_0 . This is the way infrared diffusion, which concerns large dipoles, is tamed by the existence of the saturation scale:

$$Q_s^2(x) \equiv \frac{1}{R_0^2(x)} \sim x^{-\lambda}. \quad (16)$$

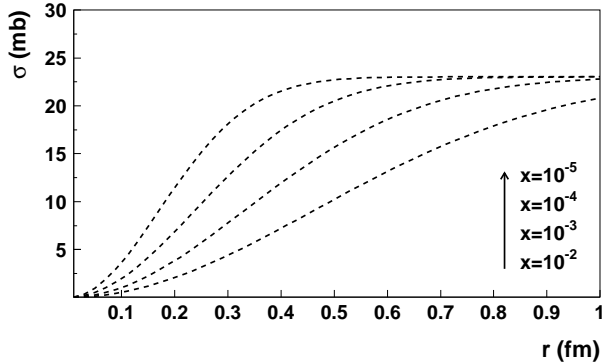


Fig. 5. The dipole cross section in the saturation model.

Thus the saturation scale rises when $x \rightarrow 0$. With the dipole cross section (14) several remarkable features of DIS data are described.

4.1. Transition to low Q^2

First, the transition to low Q^2 values in the proton structure function. This has an intuitive physical interpretation if we relate the saturation radius to the mean transverse distance between partons. If the partonic system is dilute and the $q\bar{q}$ dipole probe with a characteristic size $1/Q$ is much smaller than the saturation radius, $1/Q \ll R_0(x)$, the logarithmic behavior is found [12,13]

$$F_2 \sim \frac{\sigma_0}{R_0^2(x)} \ln(Q^2 R_0^2(x)). \quad (17)$$

In the opposite case, when $1/Q \gg R_0(x)$, the parton system looks dense for the probe and

$$F_2 \sim Q^2 \sigma_0 \ln\left(\frac{1}{Q^2 R_0^2(x)}\right). \quad (18)$$

This transition is shown in Fig. 6 for $\sigma_{\gamma^*p} = \sigma_T + \sigma_L \sim F_2/Q^2$. With a nonzero quark mass in the $q\bar{q}$ dipole even the photoproduction data can be described, which reflects a kind of continuity in the proposed description. The transition region between the two regimes, defined by the condition (critical line in the (x, Q^2) -plane)

$$Q^2 R_0^2(x) = 1 \quad (19)$$

is found to be around $Q^2 = 1 \text{ GeV}^2$ at HERA kinematics (the solid line across the model curves in Fig. 6). The critical line also indicates the limit of validity of the twist expansion (4) in the (x, Q^2) -plane [14]. It is also

interesting to analyze the energy dependence resulting from the saturation model. If this is done for increasing Q^2 values, smooth transition between the soft ($F_2 \sim x^{-0.08}$) and hard pomeron ($F_2 \sim x^{-0.3}$) values is found [12].

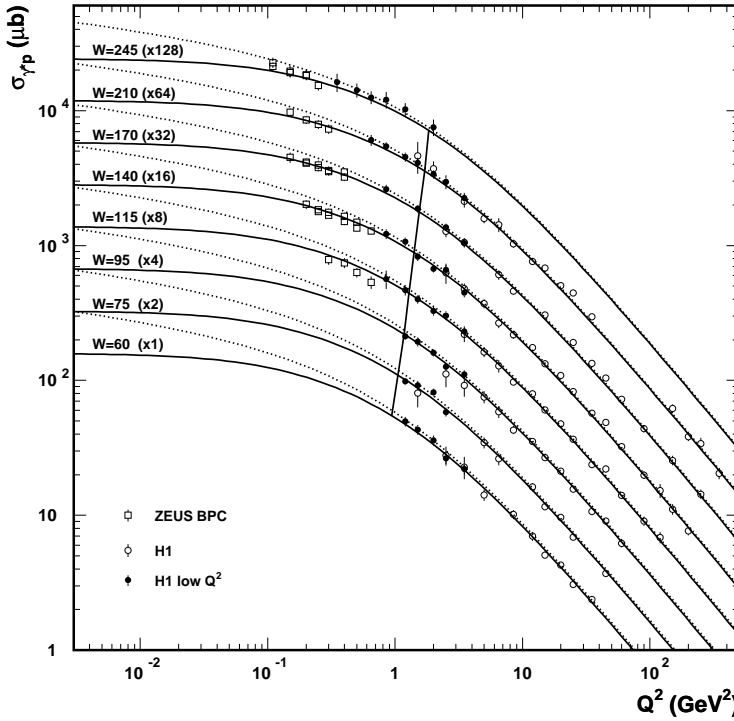


Fig. 6. The cross section $\sigma_{\gamma^*p} = \sigma_T + \sigma_L$ for fixed γ^*p center-of-mass energy W ($x = Q^2/W^2$). The dotted lines, for which $m_q = 0$, show the effect of the dipole quark mass $m_q = 140$ MeV.

4.2. DIS diffraction

Secondly, once the dipole cross section is determined from the inclusive data analysis, it can be used as a prediction for diffractive DIS [15] since for the $q\bar{q}$ pair in the diffractive final state

$$\frac{d\sigma_{T,L}^D}{dt} \Big|_{t=0} = \frac{1}{16\pi} \int d^2\mathbf{r} dz \left| \Psi_{T,L}(\mathbf{r}, z) \right|^2 \hat{\sigma}^2(x, \mathbf{r}). \quad (20)$$

The total diffractive cross section $\sigma_{\gamma^*p}^D = \sigma_T^D + \sigma_L^D$ is found after dividing (20) by the diffractive slope B_D , taken from the experiment. A very important result of the saturation model is that with the form (14), the constant ratio as a function of Q^2 and x of the diffractive and inclusive cross sections is

naturally explained [13],

$$\frac{\sigma_{\gamma^*p}^D}{\sigma_{\gamma^*p}} \sim \frac{1}{\ln(Q^2 R_0^2(x))}. \tag{21}$$

With the diffractive $q\bar{q}$ and $q\bar{q}g$ components, the description of the diffractive data is quite satisfactory, see Fig. 7 [15].

The diffractive interactions are very important for tracing saturation effects since they are mainly sensitive to intermediate dipole sizes, $r > 2/Q$, which directly probe the saturation part of the dipole cross section. In the inclusive diffractive cross section, in contrast to the fully inclusive case, the $r < 2/Q$ contribution is suppressed by additional power of $1/Q^2$ [13,15].

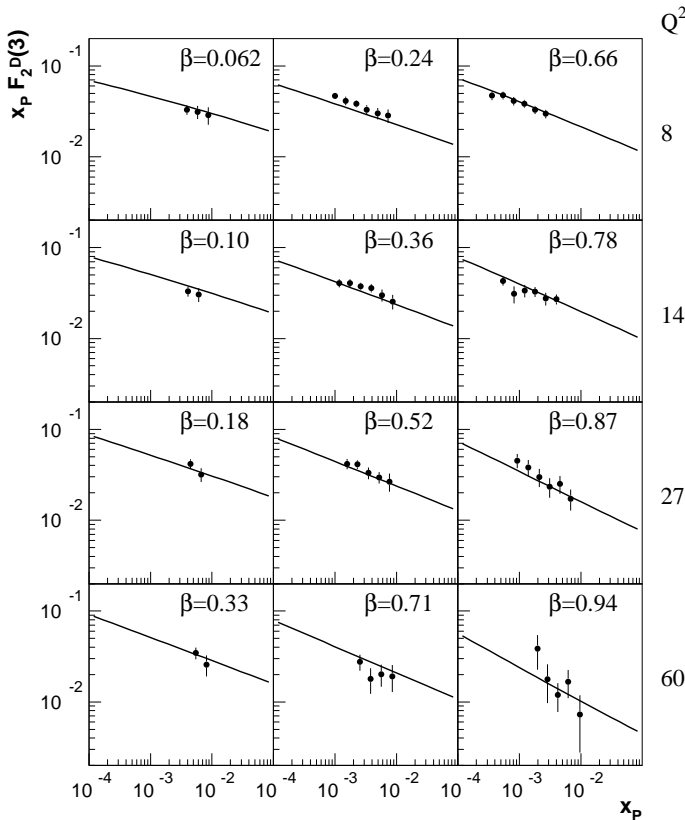


Fig. 7. The diffractive data from ZEUS [16] against the saturation model curves.

It is interesting to look at the Regge limit, $x \rightarrow 0$ and Q^2 fixed. From (18), the saturation model leads to

$$F_2 \sim Q^2 \ln \left(\frac{1}{x} \right), \quad (24)$$

which is in accord with the Froissart bound, straightforwardly applied to DIS: $F_2 \leq c \ln^2(1/x)$. The logarithm in (24) comes from the wave function Ψ_T in Eq. (10), thus there is still room for additional logarithmic dependence on x of the dipole cross section.

5. Nonlinear evolution equations

The phenomenological success of the model (14) raises the question about its relation to QCD. In particular, to what extent is the transition to saturation justified by perturbative QCD? The saturation scale $Q_s^2(x) \simeq 1 \text{ GeV}^2$ for $x \sim 10^{-4}$, thus we hope that at least the onset of saturation could be described by weakly coupled QCD.

The problem of saturation effects was attacked by Kovchegov in the dipole picture [18]. He found in the large N_c limit a nonlinear equation which is a special case of more general hierarchy of equations derived by Balitsky [19]. Strictly speaking, the derived equation is only justified for a scattering on a large nucleus since a certain class of diagrams, which could be relevant for the proton, is suppressed for DIS on a nucleus. However, this equation can be considered as a QCD model for ep DIS at small x . The basic quantity in Kovchegov's formulation is the forward scattering amplitude of the $q\bar{q}$ dipole (originated from the virtual photon) on a nucleus, $N(\mathbf{r}, \mathbf{b}, Y)$. If \mathbf{x} and \mathbf{y} are the transverse positions of the dipole quarks with respect to the center of the nucleus then $\mathbf{r} = \mathbf{x} - \mathbf{y}$ and $\mathbf{b} = (\mathbf{x} + \mathbf{y})/2$, where the latter quantity is the impact parameter of the dipole. The dipole cross section is given by

$$\hat{\sigma}(\mathbf{r}, x) = 2 \int d^2\mathbf{b} N(\mathbf{r}, \mathbf{b}, Y). \quad (25)$$

Comparing Eq. (25) with Eq. (14), we see that in the saturation model the following hypothesis on the form of N is made

$$N(\mathbf{r}, \mathbf{b}, Y) = \left\{ 1 - \exp \left(-\frac{r^2}{4R_0^2(x)} \right) \right\} \Theta(b - b_0), \quad (26)$$

where $\sigma_0 = 2\pi b_0^2$. The theta function can also be shifted into the argument of the exponent. Physically, the saturation model corresponds to the proton being a disk in the transverse plane with a sharp boundary. Any edge

effects are ignored. Saturation leads to a uniform blackening of the disk with decreasing x (for the parent dipole of a fixed size r) without changing the disk size, see Fig. 9.

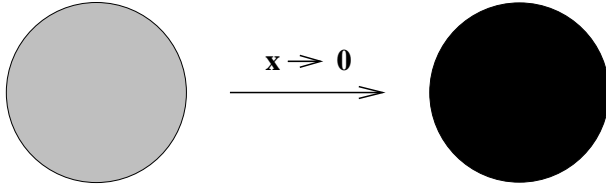


Fig. 9. Saturation (blackening) in the saturation model. Black means $\hat{\sigma} = \sigma_0$.

In the approach of Kovchegov the amplitude, $N(\mathbf{r}, \mathbf{b}, Y)$ is determined dynamically from the nonlinear evolution equation derived in the large N_c limit. Transforming back into the momentum representation

$$\phi(\mathbf{k}, \mathbf{b}, Y) = \int \frac{d^2\mathbf{r}}{2\pi} \exp(-i\mathbf{k} \cdot \mathbf{r}) \frac{N(\mathbf{r}, \mathbf{b}, Y)}{r^2}, \tag{27}$$

the following equation is found for small dipoles $r \ll 1/\Lambda_{\text{QCD}}$

$$\frac{\partial \phi(\mathbf{k}, \mathbf{b}, Y)}{\partial Y} = (K \otimes \phi)(\mathbf{k}, \mathbf{b}, Y) - \bar{\alpha}_s \phi^2(\mathbf{k}, \mathbf{b}, Y), \tag{28}$$

where $\bar{\alpha}_s = N_c \alpha_s / \pi$ and K is the kernel of the linear BFKL equation [18]. In the dipole picture in the leading $\ln(1/x)$ approximation, the above equation describes not only the production but also merging of dipoles in the dipole cascade. In addition, an energy independent initial condition for the evolution is supplied at $Y = Y_0$ which describes the scattering of the parent $q\bar{q}$ dipole off the nucleons through multiple two-gluon color singlet exchange [20]. The effect of the nonlinear evolution equation is the generation of the interacting dipole cascade which brings the energy dependence of the solution. In terms of Feynman diagrams, Eq. (28) resumes fan diagrams with the BFKL ladders and triple pomeron couplings in the large N_c limit [21], see Fig. 10.

Assuming the sharp disk model for the b -dependence, both analytical and numerical studies of Eq. (28) [18, 21–24] confirm the picture of blackening, anticipated in the saturation model. The dipole cross section (25) computed after solving Eq. (28) features color transparency for small r and saturation at large r with a similar dependence on x , *i.e.* for smaller x the saturation occurs for smaller dipole sizes. Moreover, the saturation scale emerges in such analysis. This is illustrated in detail in Fig. 11 where the solution $\phi(k, Y)$ of Eq. (28) (solid lines) and the solution of the corresponding linear BFKL equation (dotted lines), projected on the (k, Y) -plane, are

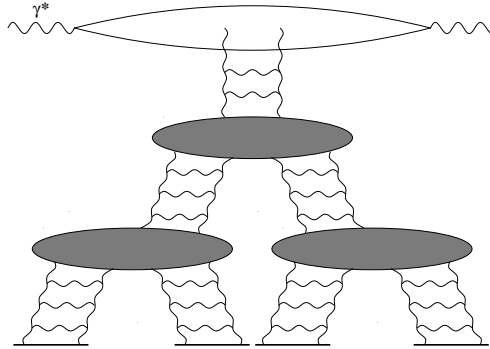


Fig. 10. The BFKL fan diagrams resummed by Eq. (28).

shown [24]. The BFKL solution exhibits diffusion into small and large values of k even though the initial condition is concentrated at $k = k_0$. The non-linear saturation effects in the equation (28) tame infrared diffusion, pulling the solution into the infrared safe region. The straight lines for the nonlinear solution reflect the scaling property: $\phi(k, Y) = \phi(k/Q_s(Y))$, where the saturation scale $Q_s(Y)$ corresponds to the central line $k = Q_s(Y)$, see [24] for more details. It is important to note that the scaling sets in independent of initial conditions and it is strictly valid for $k < Q_s(Y)$. For $k > Q_s(Y)$,

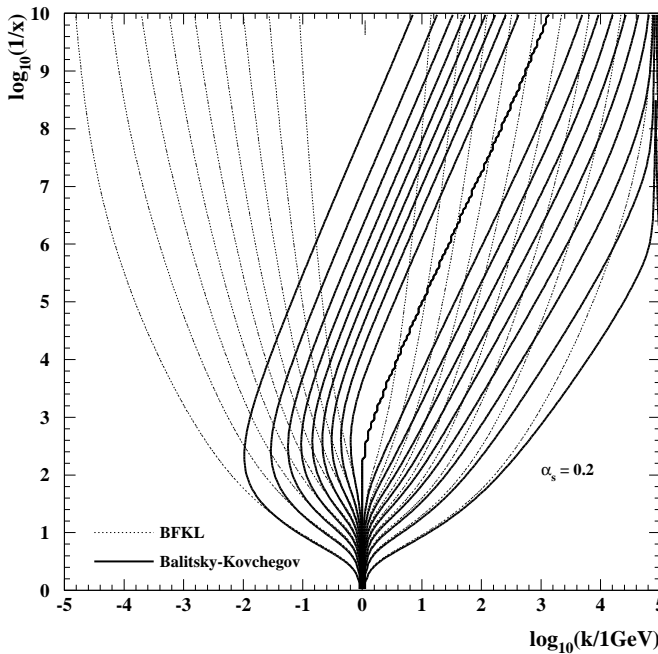


Fig. 11. Diffusion in the BFKL and Balitsky–Kovchegov equations.

however, the scaling is mildly violated. This was analyzed recently in [25] where the region of validity of geometric scaling was found.

Unfortunately, the agreement between the results based on the Eq. (28) and the saturation model is only qualitative and detailed studies of the DIS data with this equation are necessary.

An intriguing question, related to proton confinement, is the impact parameter dependence of the dipole–proton forward scattering amplitude $N(\mathbf{r}, \mathbf{b}, Y)$. Certainly, the sharp disk picture with a fixed boundary is oversimplified if not questionable. Recently, detailed studies with Eq. (28) in the \mathbf{r} -representation were done [26], assuming the initial condition $N(\mathbf{r}, \mathbf{b}, Y_0) = N(\mathbf{r}) S(\mathbf{b})$ with some nonperturbative profile function $S(\mathbf{b})$ which falls as $\exp(-2m_\pi b)$ at large b . The result of this analysis is shown in Fig. 12. The black disk corresponds to saturation but now the saturation area rises according to the nonlinear evolution equation (28) (or the equation of the Color Glass Condensate [27]) when $x \rightarrow 0$. Thus for each impact parameter b unitarity limit is achieved. The grey area corresponds to lower parton densities where the linear BFKL equation applies. Within this approach the Froissard bound is saturated: $F_2 \sim \ln^2(1/x)$.

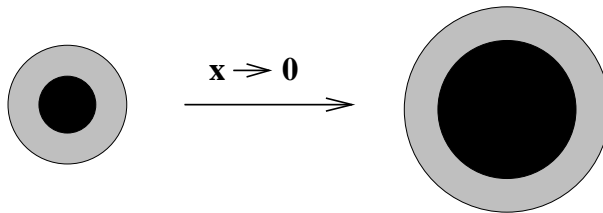


Fig. 12. Black disk expansion and saturation.

The impact parameter dependence of the forward scattering amplitude can be studied through the t -dependence of diffractive vector meson production in DIS [28], see Fig. 13. In this model, the vector meson production is a three step process, the virtual photon splits into the $q\bar{q}$ pair which interacts with the proton with the amplitude $A_{el}^{q\bar{q}-p}$, and then forms a meson described by the wave function Ψ_V ,

$$\frac{d\sigma_V}{dt} = \frac{1}{16\pi} \left| \int d^2\mathbf{r} dz \bar{\Psi}_{\gamma^*}(Q^2, \mathbf{r}, z) A_{el}^{q\bar{q}-p}(\mathbf{r}, \mathbf{\Delta}, x) \Psi_V(M_V, \mathbf{r}, z) \right|^2 \quad (29)$$

where M_V is the vector meson mass, and the amplitude

$$A_{el}^{q\bar{q}-p}(\mathbf{r}, \mathbf{\Delta}, x) = 2 \int d^2\mathbf{b} N(\mathbf{r}, \mathbf{b}, x) e^{i\mathbf{b}\cdot\mathbf{\Delta}} \quad (30)$$

and $\mathbf{\Delta}$ is a two dimensional vector of transverse momentum transferred from the proton into the $q\bar{q}$ system, $t = -\mathbf{\Delta}^2$ Qualitatively, the presented above

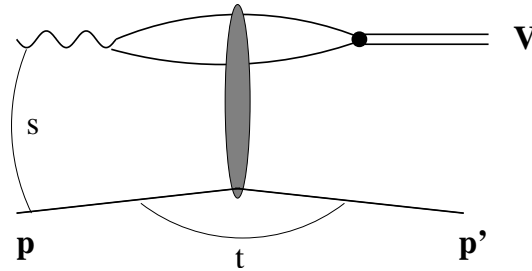


Fig. 13. Diffractive vector meson production.

results are confirmed although the proton is not fully black at the central impact parameter $b = 0$ in HERA kinematics. We would like to stress that diffractive vector meson production in $\gamma^* p$ scattering is potentially the best process to study saturation effects in DIS since the transverse size of the $q\bar{q}$ pair forming a meson is controlled by the vector meson mass

$$\bar{r} = \frac{1}{\sqrt{M_V^2 + Q^2}}. \quad (31)$$

Thus we expect saturation effects to be more important for larger (lighter) vector mesons. The first analysis in this direction done in [29] with the saturation model seems to confirm this observation.

Let us finish by pointing out that the nonlinear equation (28) is obtained in the closed form due to the large N_c limit assumption. In general, in the leading $\ln(1/x)$ approximation, a hierarchy of nonlinear equations is found by Balitsky [19]. These equations, written in a closed form by Weigert [30], are equivalent to the Color Glass Condensate renormalization group equation [27], see [32] for details and more references. A similar equation to Eq. (28) was also derived for diffractive DIS [33]. A different approach to unitarization at small x relies on the summation of interacting reggeized gluons [34], forming a compound color singlet state. The BFKL equation is obtained assuming two exchanged reggeized gluons. Recently, an energy spectrum of the scattering amplitude in high energy asymptotics with up to eight reggeized gluons was found in the large N_c limit [35]. For the discussion of the relation between the approach based on multiple BFKL pomeron exchanges leading to Eq. (28), and the approach based on exchanged reggeized gluons, see [36].

6. Conclusions and outlook

We presented basic concepts of parton saturation. This phenomenon arises in DIS at small x which is characterized by a strong rise of parton

densities in the nucleon. However, the strong rise is tamed in accordance with unitarity of the description by the interactions between partons (mostly gluons). As a result, gluons form a coherent system characterized by the saturation scale. The distribution of gluons with the transverse momentum below this scale no longer strongly rises. This effects are important not only in ep DIS but also in nucleus–nucleus collisions studied at RHIC [31].

Formulated in the dipole picture, the saturation effects impose strong bound on the form of the dipole–proton cross section for the dipole sizes bigger than the inverse of the saturation scale. This feature was build in the phenomenological model [12] of the dipole cross section which successfully describes the inclusive and diffractive DIS data from HERA. In addition, based on the existence of the saturation scale, the new scaling (“geometric scaling”) was proposed and successfully confronted with the data. The QCD based attempt to justify the main features of the phenomenological description, which gives rise to a formulation of a nonlinear evolution equation, was presented. Based on the numerical solution to this equation we showed the main effect of saturation which suppresses diffusion into small values of transverse gluon momenta, present in the approach based on the linear BFKL equation. We also discussed the relevance of the impact parameter studies which touch the problem of proton confinement. Experimentally, this is done through the diffractive vector meson production.

From the theoretical side, the future work will concentrate on detailed analysis of nonlinear equations describing parton saturation. Refraining from the large N_c limit, there are two equivalent formulations, the Color Glass Condensate equation [27] and the equation derived by Weigert [30] which beautifully summarizes the infinite hierarchy of the equations obtained by Balitsky [19]. It would be good to have full handle over these equations.

From the phenomenological side, more precise data awaited from HERA II will allow to test the parton saturation formulations in great detail. For this purpose, the phenomenological saturation model (14) was refined in order to include the DGLAP gluon evolution, expected at small r [37]. All important features of the saturation in the original model, however, were retained.

The attractiveness of the presented description of saturation effects to large extent relies on the dipole formulation (10) obtained in the leading $\ln(1/x)$ approximation. How this picture will change when the next-to-leading order corrections to the formula (5) are computed which introduce the $q\bar{q}g$ Fock state in the photon wave function in the dipole formulation, is not known yet. The computations are under way [38].

This paper was supported in part by the Polish State Committee for Scientific Research (KBN) grant no. 5 P03B 144 20 and by the Deutsche Forschungsgemeinschaft.

REFERENCES

- [1] V.N. Gribov, L.N. Lipatov, *Sov. J. Nucl. Phys.* **15**, 438 (1972); G. Altarelli, G. Parisi, *Nucl. Phys.* **B126**, 298 (1977); Yu.L. Dokshitzer, *Sov. Phys. JETP* **46**, 641 (1977).
- [2] S. Catani, M. Ciafaloni, F. Hautmann, *Phys. Lett.* **B242**, 97 (1990); *Nucl. Phys.* **B366**, 657 (1991); J.C. Collins, R.K. Ellis, *Nucl. Phys.* **B360**, 3 (1991); E.M. Levin, M.G. Ryskin, Yu.M. Shabel'sky, A. Shuvaev, *Sov. J. Nucl. Phys.* **53**, 657 (1991).
- [3] L.N. Lipatov, *Sov. J. Nucl. Phys.* **23**, 338 (1976); E.A. Kuraev, L.N. Lipatov, V.S. Fadin, *Sov. Phys. JETP* **44**, 443 (1976); *Sov. Phys. JETP* **45**, 199 (1977); Ya.Ya. Balitsky, L.N. Lipatov, *Sov. J. Nucl. Phys.* **28**, 338 (1978).
- [4] V. Fadin, *BFKL news*, Talk given at LISHEP 98, Rio de Janeiro, Brazil, 16–20 Feb. 1998, hep-ph/9807528; G.P. Salam, *Acta Phys. Pol.* **30**, 3679 (1999).
- [5] L.V. Gribov, E.M. Levin, M.G. Ryskin, *Phys. Rep.* **100**, 1 (1983).
- [6] A.H. Mueller, Jian-wei Qiu, *Nucl. Phys.* **B268**, 427 (1986).
- [7] J.C. Collins, J. Kwieciński, *Nucl. Phys.* **B335**, 89 (1989); J. Bartels, G. Levin, *Nucl. Phys.* **B387**, 617 (1992); L. McLerran, R. Venugopalan, *Phys. Rev.* **D49**, 2233 (1994); *Phys. Rev.* **D49**, 3352 (1994); *Phys. Rev.* **D50**, 2225 (1994).
- [8] J.R. Forshaw, D.A. Ross, *Quantum Chromodynamics and the Pomeron*, Cambridge University Press, England, Cambridge 1996.
- [9] J.D. Bjorken, J.B. Kogut, D.E. Sopper, *Phys. Rev.* **D3**, 1382 (1970).
- [10] A.H. Mueller, *Nucl. Phys.* **B415**, 373 (1994); *Nucl. Phys.* **B437**, 107 (1995); A.H. Mueller, B. Patel, *Nucl. Phys.* **B425**, 471 (1994); Z. Chen, A.H. Mueller, *Nucl. Phys.* **B451**, 579 (1995).
- [11] N.N. Nikolaev, B.G. Zakharov, *Z. Phys.* **C64**, 651 (1994); *Sov. Phys. JETP* **78**, 598 (1994).
- [12] K. Golec-Biernat, M. Wüsthoff, *Phys. Rev.* **D59**, 014017 (1999).
- [13] K. Golec-Biernat, *J. Phys. G* **28**, 1057 (2002).
- [14] J. Bartels, K. Golec-Biernat, K. Peters, *Eur. Phys. J.* **C17**, 121 (2000).
- [15] K. Golec-Biernat, M. Wüsthoff, *Phys. Rev.* **D60**, 114023 (1999), *Eur. Phys. J.* **C20**, 313 (2001).
- [16] ZEUS Collaboration, M. Derrick *et al*, *Eur. Phys. J.* **C6**, 43 (1999).
- [17] A.M. Staśto, K. Golec-Biernat, J. Kwieciński, *Phys. Rev. Lett.* **B86**, 596 (2001).
- [18] Yu.V. Kovchegov, *Phys. Rev.* **D60**, 034008 (1999); *Phys. Rev.* **D61**, 074018 (2000).
- [19] I. Balitsky, *Nucl. Phys.* **B463**, 99 (1996); hep-ph/0101042.
- [20] A.H. Mueller, *Nucl. Phys.* **B335**, 115 (1990).
- [21] M.A. Braun, *Eur. Phys. J.* **C16**, 337 (2000); N. Armesto, M.A. Braun, *Eur. Phys. J.* **C20**, 517 (2001).

- [22] E. Levin, K. Tuchin, *Nucl. Phys.* **B573**, 833 (2000); *Nucl. Phys.* **A691**, 779 (2001); *Nucl. Phys.* **A693**, 787 (2001).
- [23] E. Levin, M. Lublinsky, *Nucl. Phys.* **A696**, 833 (2001); M. Lublinsky, *Eur. Phys. J.* **C21**, 513 (2001).
- [24] K. Golec-Biernat, L. Motyka, A.M. Staśto, *Phys. Rev.* **D65**, 074037 (2002).
- [25] J. Kwieciński, A.M. Staśto, [hep-ph/0203030](#); E. Iancu, K. Itakura, L. McLerran, [hep-ph/0203137](#); E. Iancu, K. Itakura, L. McLerran, [hep-ph/0205198](#).
- [26] E. Ferreiro, E. Iancu, K. Itakura, L. McLerran, [hep-ph/0206241](#).
- [27] E. Iancu, A. Leonidov, L. McLerran, *Nucl. Phys.* **A692**, 583 (2001); *Phys. Lett.* **B510**, 133 (2001); E. Ferreiro, E. Iancu, A. Leonidov, L. McLerran, *Nucl. Phys.* **A703**, 489 (2002).
- [28] S. Munier, A.M. Staśto, A.H. Mueller, *Nucl. Phys.* **B603**, 427 (2001); S. Munier, [hep-ph/0206117](#).
- [29] A.C. Caldwell, M.S. Soares, *Nucl. Phys.* **A696**, 125 (2001).
- [30] H. Weigert, *Nucl. Phys.* **A703**, 823 (2002).
- [31] L. McLerran, [hep-ph/0202025](#).
- [32] J.-P. Blaizot, E. Iancu, H. Weigert, [hep-ph/02060779](#).
- [33] Yu. V. Kovchegov, E. Levin, *Nucl. Phys.* **B577**, 221 (1999).
- [34] J. Bartels, *Nucl. Phys.* **B175**, 365 (1980); J. Kwieciński, M. Praszalowicz, *Phys. Lett.* **B94**, 413 (1980).
- [35] G.P. Korchemsky, J. Kotański, A.N. Manashov, *Phys. Rev. Lett.* **88**, 122002 (2002); J. Kotański, *Acta Phys. Pol.* **B33** (2002), next issue.
- [36] Yu.V. Kovchegov, [hep-ph/020223](#).
- [37] J. Bartels, K. Golec-Biernat, H. Kowalski, *Phys. Rev.* **D66**, 014001 (2002); *Acta Phys. Pol.* **B33**, 2853 (2002).
- [38] S. Gieseke, *Acta Phys. Pol.* **B33**, 2873 (2002).